Vibrational Analysis of Crystalline Tri-L-Alanine*

WEILI QIAN,† JAGDEESH BANDEKAR,‡ and SAMUEL KRIMM

Biophysics Research Division and Department of Physics, University of Michigan, Ann Arbor, Michigan 48109

SYNOPSIS

We have found that tri-L-alanine (Ala_3) can crystallize in a parallel-chain β structure in addition to the previously known antiparallel-chain β structure. Although the chain conformations in each structure are essentially similar, the ir and Raman spectra are distinctively different. We have calculated the normal modes of each structure, and can account in significant detail for these differences. This demonstrates the essential validity of our empirically refined force fields, as well as showing that deeper insights into polypeptide and protein structure can be achieved through the rigorous analyses of normal mode calculations.

INTRODUCTION

Tri-L-alanine (Ala_3) has been shown to inhibit the esterolytic activity of elastase.[1] It may therefore be useful to understand the vibrational dynamics of this tripeptide in some detail in order to be able to investigate its interaction with the enzyme.

We initiated such a study by analyzing the vibrational spectrum of crystalline Ala_3. Its three-dimensional structure had been determined,[2] and it was shown that its molecules pack so that the hydrogen bonds between peptide groups form an antiparallel-chain pleated sheet arrangement, Ala_3 (AP). However, instead of the needle-shaped crystals found in the x-ray study,[2] we obtained large platelet crystals, the crystal form, as we subsequently determined, being dependent on the solvent from which the material is crystallized. Spectra of this second crystal form were found to be different, and subsequent crystallographic analysis[3] has shown that the Ala_3 molecules in the platelet crystals pack so that the hydrogen bonds between peptide groups form a parallel-chain sheet arrangement, Ala_3 (P).

These two very different crystal structures for the same molecule thus provide sensitive tests of our force field for the polypeptide chain[4] and our dipole derivatives to calculate ir intensities.[5] We have therefore performed detailed normal mode analyses, and ir and Raman spectral assignments, for the two crystal structures.

EXPERIMENTAL PROCEDURES

Crystals of Ala_3 were grown from dimethylformamide (DMF)–water mixtures. We found that if the ratio by volume of DMF : H_2O is 20 : 80 or less, the crystals grown by slow evaporation of solvent are colorless needles. The crystal structure of this form has been reported,[2] and consists of Ala_3 molecules in an antiparallel-chain pleated-sheet arrangement with one molecule of water of crystallization for every two Ala_3 molecules (see Figure 1). However, when the ratio of DMF : H_2O is more than 20 : 80, large platelets are obtained (ours were about $4 \times 2 \times 0.4$ mm), which are found[3] to have Ala_3 molecules in a parallel-chain sheet arrangement without any water of crystallization (see Figure 2). Deuteration of the molecules was done by repeated treatment with DMF/D_2O. After several cycles, exchange seemed to be complete, as judged by the absence of NH stretch bands in the Raman spectrum. The ir spectra, however, run on KBr pellets, showed evidence of incomplete deuteration, or possibly of re-exchange. Since the deuteration was nevertheless

Biopolymers, Vol. 31, 193–210 (1991)
 CCC 0006-3525/91/020193-18$04.00

* This paper is number 41 in a series on vibrational analysis of peptides, polypeptides, and proteins, of which Ref. 15 is paper 40.

† Present address: Department of Chemistry, University of South Carolina, Columbia, SC 29208.

‡ Present address: BOC Group Technical Center, 100 Mountain Avenue, Murray Hill, NJ 07974.

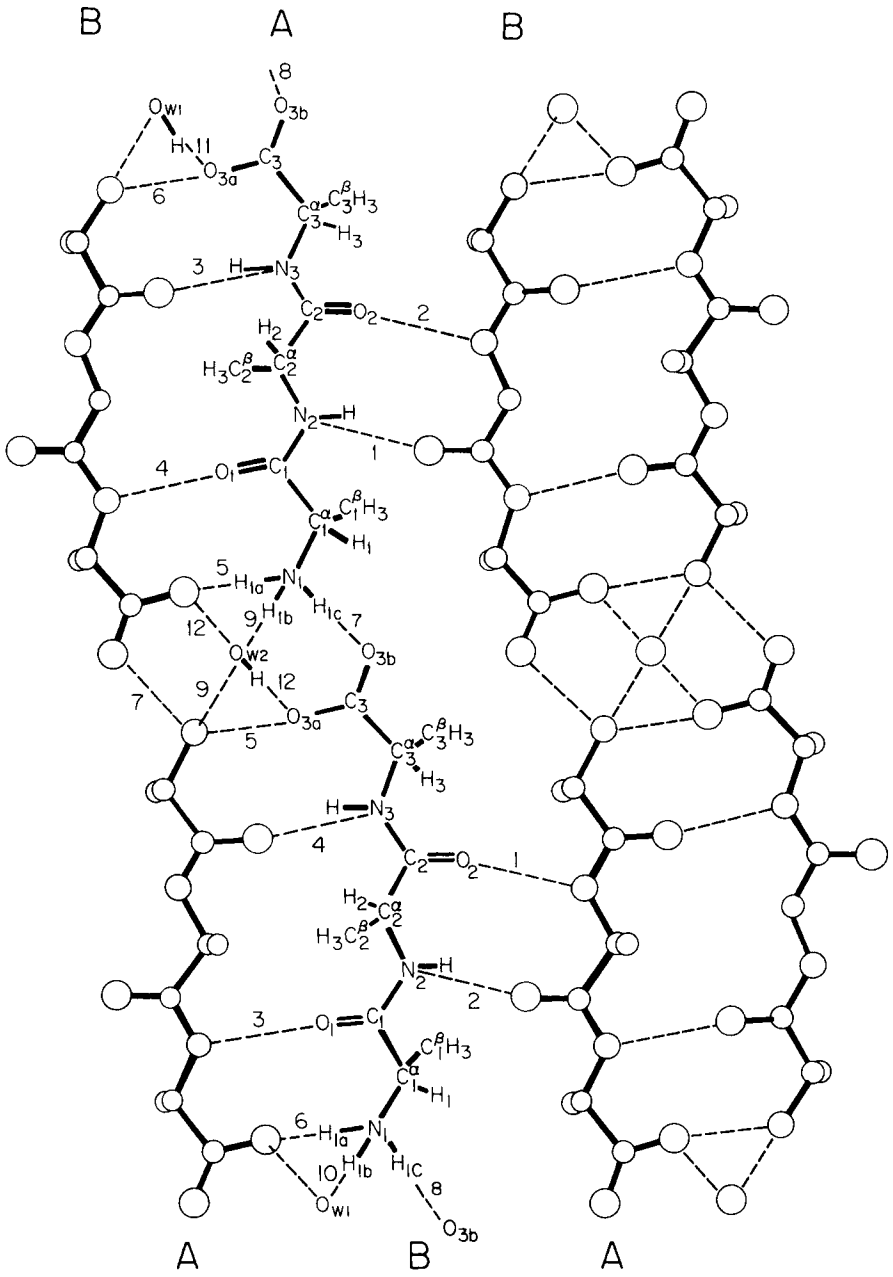

Figure 1. Arrangement of tri-L-alanine molecules in hydrogen-bonded sheets of the antiparallel-chain crystal structure.[2] Chain atoms and hydrogen bonds (---) of Ala_3(AP) are numbered as referred to in text and tables.

extensive, we have used such spectra for guidance in making assignments, aided by normal mode calculations on the fully deuterated molecules.

Infrared spectra of both types of crystals were obtained on a Bomem DA-3 Fourier transform ir spectrometer, at 2 cm^{-1} resolution, and are shown in Figure 3 for Ala_3(AP) and its N-deuterated derivative, Ala_3(AP)-ND. Raman spectra were obtained on a Spex 1403 spectrometer with Ar^+ laser 514.5 nm excitation, at 2 cm^{-1} resolution, and comparable spectra for Ala_3(AP) are shown in Figure 4. Infrared and Raman spectra of Ala_3(P) and Ala_3(P)-ND are shown in Figures 5 and 6, respectively.

NORMAL MODE CALCULATIONS

Structure

The unit cell of Ala_3(AP) is monoclinic, space group C2, with a = 18.513 Å, b = 5.330 Å, c = 24.775 Å, β

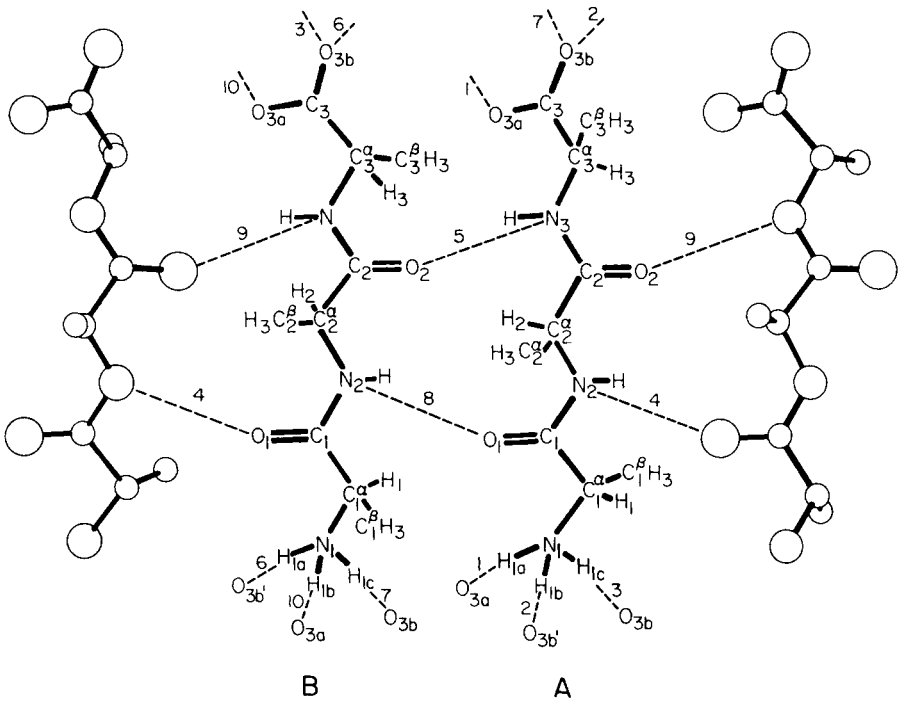

Figure 2. Arrangement of tri-L-alanine molecules in hydrogen-bonded sheets of the parallel-chain crystal structure.[3] Chain atoms and hydrogen bonds (---) of $Ala_3(P)$ are numbered as referred to in text and tables.

= 98.64°, and $Z = 8$.[2] There are two molecules in the asymmetric unit (see Figure 1), and the primitive cell contains 4 molecules, the second A,B pair being related to the first by a twofold axis parallel to *b* and passing through the water molecules. This results in an antiparallel-chain arrangement with hydrogen bonds between peptide groups in sheets in the *ac* plane. The methyl side groups project alternately above and below these planes. The interpeptide hydrogen bonds are significantly weaker than those involving the terminal NH_3^+ groups.[2]

The unit cell of $Ala_3(P)$ is monoclinic, space group $P2_1$, with $a = 9.862$ Å, $b = 10.004$ Å, $c = 11.849$ Å, $\beta = 101.3°$, and $Z = 4$.[3] There are two molecules in the asymmetric unit: A and B in Figure 2 are not related by a translation, but are slightly twisted about their axes with respect to each other. The primitive unit cell contains 4 molecules: alternate sheets of parallel-chain hydrogen-bonded molecules (in the *ac* plane) have opposite orientations of molecules. There is no water of crystallization. The interpeptide hydrogen bonds are even weaker than those in $Ala_3(AP)$, with the strong hydrogen bonds linking end groups within sheets (1, 3, 7, and 10) and between sheets (2 and 6).

In order to transfer our polypeptide force field for β-poly(L-alanine) (β-PLA)[6,7] to Ala_3, it is necessary to use standard bond lengths and angles as well as planar peptide groups.[4] We therefore generated crystal structures with such standard parameters but with the dihedral angles of the original structures.[2,3] The bond lengths and angles for the end groups were obtained as follows. Structural studies using neutron diffraction techniques have been reported on glycine,[8] L-alanine,[9] L-serine,[10] and L-cysteine.[11] We used the mean values from these reports for the following parameters: $d(C\text{-}O^-) = 1.249$ Å, $d(N\text{-}H^+) = 1.037$ Å; angles around the N of NH_3^+ were assumed to be tetrahedral; the angles $C_3^\alpha CO^-$ and OC_3O were taken to be 117.23° and 125.6°, respectively. The dihedral angles $\tau(H\text{-}N_1\text{-}C_1^\alpha\text{-}C_1)$ were taken to be 120.0°, 0°, and −120.0°, and the dihedral angles $\tau(N_3\text{-}C_3^\alpha\text{-}C_3\text{-}O_{3a})$ and $\tau(N_3\text{-}C_3^\alpha\text{-}C_3\text{-}O_{3b})$ were taken[9] to be −18.6° and 161.5°, respectively. Hydrogen bonding to water molecules was approximated by using pendant atoms.

Force Field

The internal and local symmetry coordinates of the peptide chain were transferred from our earlier work on β-PLA.[6,7] As was done in the case of L-Val-Gly-Gly,[12] the CO_2^- wagging coordinate of the planar $C_3^\alpha C_3OO^-$ group was defined as an out-of-plane bend by $\Delta\omega = \Delta\alpha \sin(OCO)$, where $\Delta\alpha$ denotes the displacement of the $C_3^\alpha C$ bond from the OCO plane.

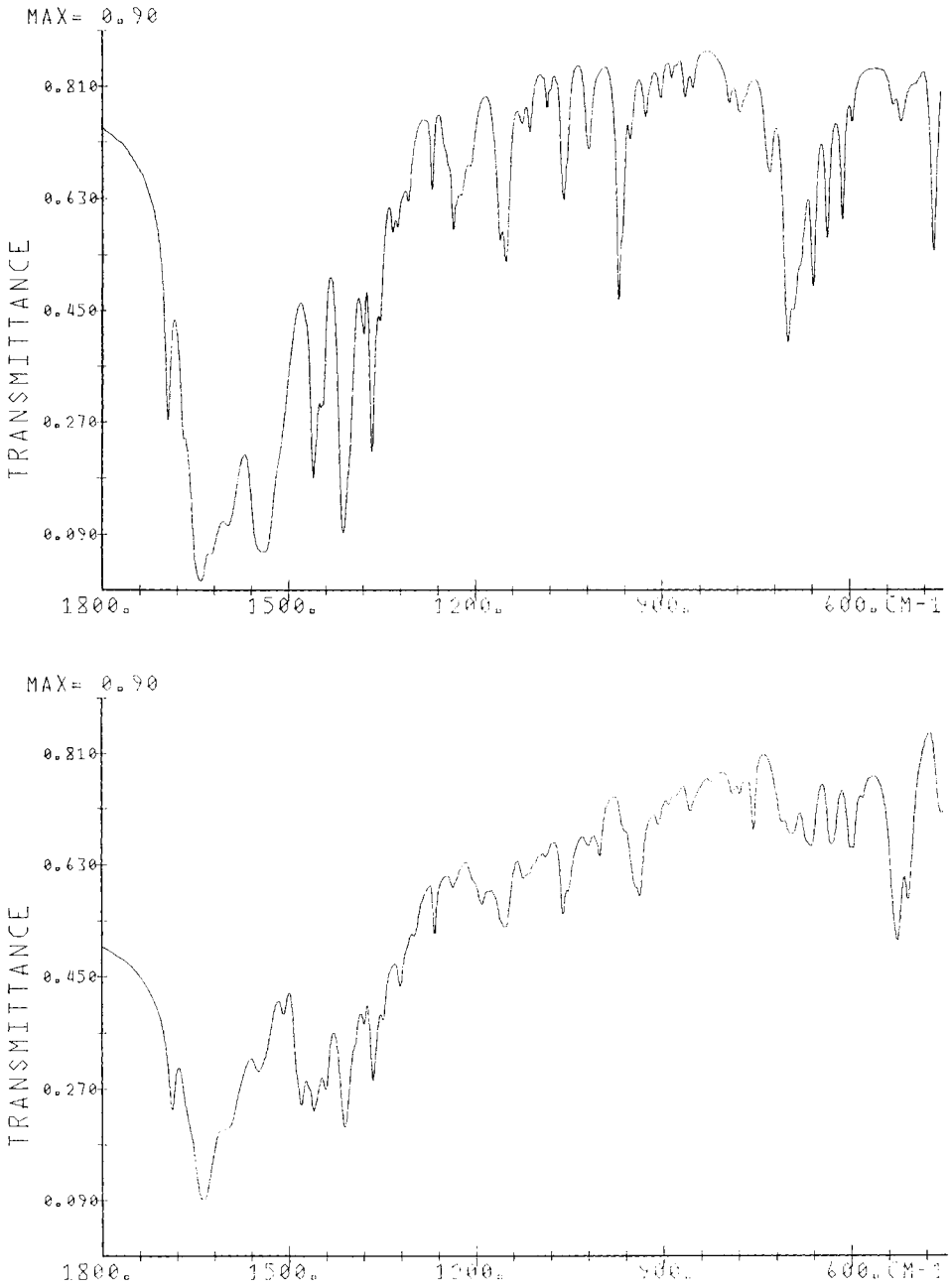

Figure 3. Infrared spectra of (a) Ala_3(AP) and (b) Ala_3(AP)-ND.

The force constants for the peptide group were transferred from the work on β-PLA.[6,7] However, because of the large variations in hydrogen-bond strengths in Ala_3, with associated variations in bond lengths, it was not possible to keep some important diagonal terms constant. This was particularly true of the C=O stretch constant, f(C=O), since the maximum variation in bond lengths is 0.015 Å, an amount that has been shown by ab initio studies to lead to very significant variations in f(C=O).[13,14] [Similar variations would be appropriate for f(NH),[13-15] and were shown to apply for Gly_3[16]; we have not implemented them here because we did not analyze this region of the spectrum in detail.] The C=O bond lengths are given in Table I, together with the values of f(C=O) that we found appropriate. The variation in f(C=O) with d(C=O) parallels that in Gly_3,[16] and is very similar to that found from ab initio studies[13,14] if the latter force constants are scaled to the values required experi-

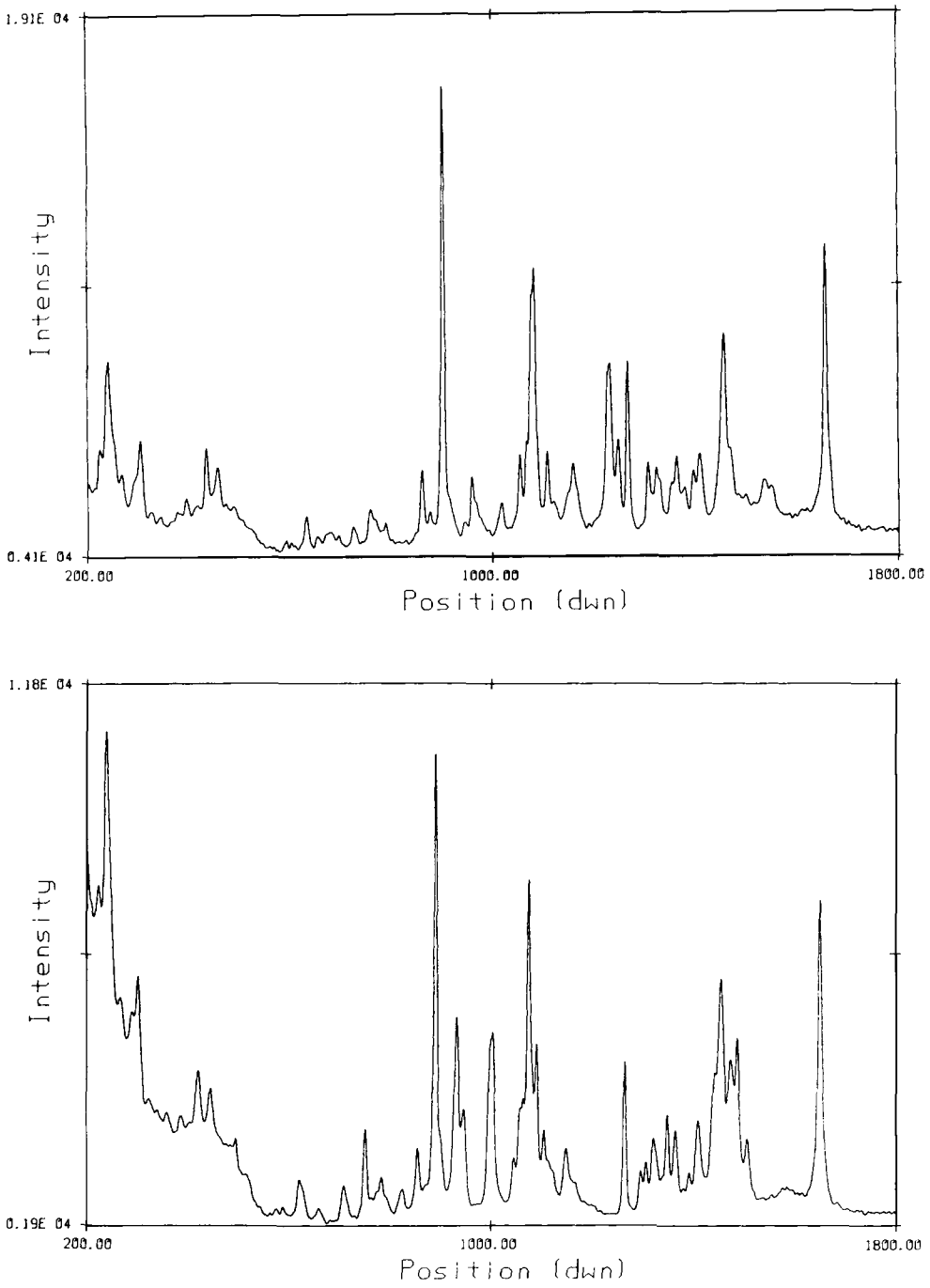

Figure 4. Raman spectra of (a) Ala_3(AP) and (b) Ala_3(AP)-ND.

mentally for Ala_3. Because of the large variation in hydrogen-bond lengths,[2,3] we also varied $f(H\cdots O)$: as we had done before,[17] we allowed $f(H\cdots O)$ to decrease linearly from its value of 0.150 mdyn $Å^{-1}$ at $d(H\cdots O)$ = 1.76 Å[18] to 0.0 mdyn $Å^{-1}$ at $d(H\cdots O)$ = 5.0 Å.

Initial values of force constants for the end groups were transferred from our analysis of L-Val-Gly-Gly[12] and Gly_3.[16] Since the end-group hydrogen bonds in Ala_3(AP) and Ala_3(P) are different, as well as being different from those in the above tripeptides, it was not possible to use a common set of force constants that would be satisfactory for both structures. We therefore refined these force constants empirically, and their values are given in Table II.

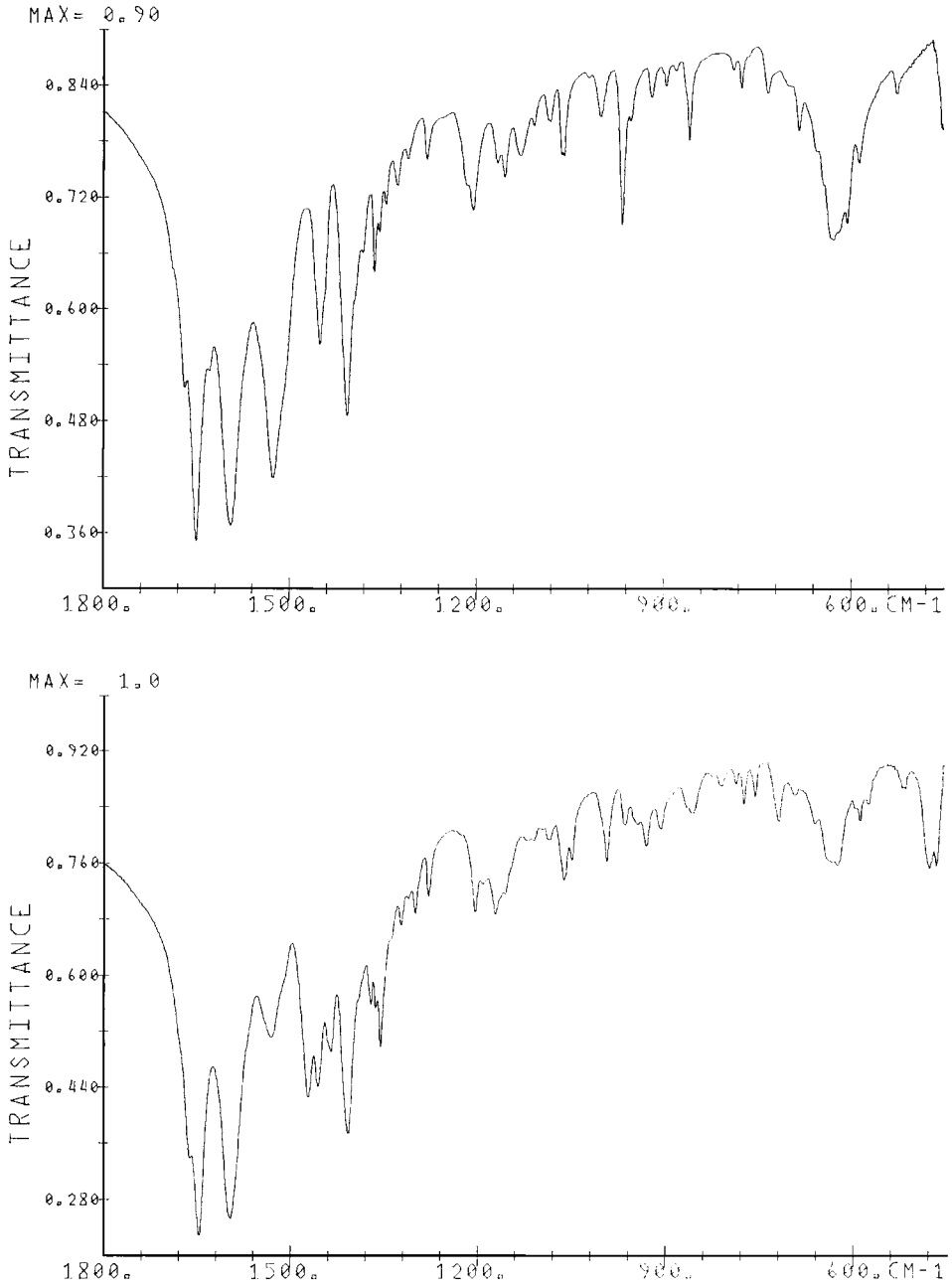

Figure 5. Infrared spectra of (a) $Ala_3(P)$ and (b) $Ala_3(P)$-ND.

Frequency shifts and ir intensities for amide I and II modes were calculated by dipole derivative coupling (DDC),[12] using dipole derivatives for the peptide group obtained from ab initio calculations of hydrogen-bonded N-methylacetamide.[5]

RESULTS AND DISCUSSION

Calculated normal mode frequencies are compared with observed Raman and ir bands in Table III for $Ala_3(AP)$ and in Table IV for $Ala_3(P)$. Although we have calculated the normal modes of the deuterated species, these are not presented in detail but will be referred to in the discussion. We do not include a detailed analysis of the NH stretch (s) and CH s modes, but will comment on these separately. Nor do we discuss the region below 200 cm^{-1}, since data are limited and the specific nature of the predicted (mostly hydrogen bond) modes depends sensitively on exact knowledge of the hydrogen-bond force constants, which is admittedly limited at this

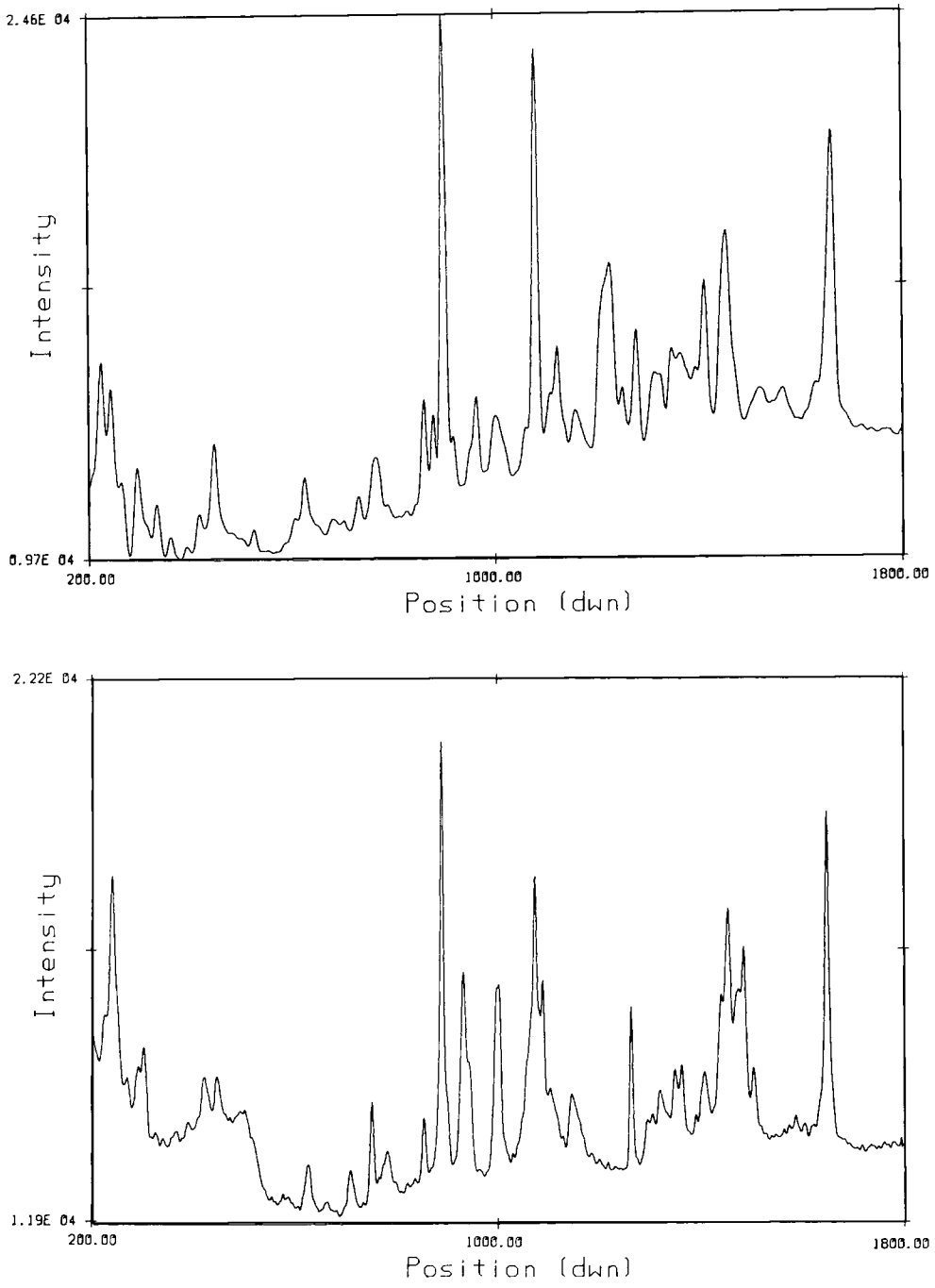

Figure 6. Raman spectra of (a) $Ala_3(P)$ and (b) $Ala_3(P)$-ND.

stage, and on nonbonded interactions in the crystal, which have not been included in the calculation. In most cases, the modes in the A and B molecules are essentially identical and of the same frequency; we have tried to assign bands with this consideration in mind. In some cases, however, the coupling between molecules is significant enough to give observable frequency splittings, and we endeavored to assign these. Of course, the frequency differences between A and B symmetry species is, as expected, minimal, since the interactions between pairs of molecules related by symmetry is relatively small, except in the low-frequency region.

In the discussion below, we will consider the assignments of modes in terms of various groupings, comparing the results for $Ala_3(AP)$ and $Ala_3(P)$ within each group. Because of the complexity of the system and the limited study of isotopic derivatives,

Table I Bond Lengths and Force Constants of C=O Groups in Ala_3

	d(C=O), Å	f(C=O), mdyn·Å^{-1}
Ala_3(AP)		
$C_1{=}O_1$(A)	1.229	9.768
$C_2{=}O_2$(A)	1.233	9.652
$C_1{=}O_1$(B)	1.233	9.652
$C_2{=}O_2$(B)	1.233	9.652
Ala_3(P)		
$C_1{=}O_1$(A)	1.220	10.030
$C_2{=}O_2$(A)	1.221	10.000
$C_1{=}O_1$(B)	1.235	9.600
$C_2{=}O_2$(B)	1.232	9.684

it will not be surprising that some assignments can be made with greater confidence than others.

Amide Modes

Amide I. The amide I modes exhibit large splittings, 43 cm^{-1} in the case of the AP structure and 32 cm^{-1} in the case of the P structure. These splittings are primarily a result of the DDC, the absence of which results in maximum splittings of 23 (AP) and 26 (P) cm^{-1}. The reason for the larger unperturbed splittings than in β-PLA, where it is 8 cm^{-1},[4] is due to the constant value of f(C=O) in the latter case compared to the variable values in Ala_3 (cf. Table I). Nevertheless, despite the much larger maximum difference in f(C=O) values for Ala_3(P) than for Ala_3(AP), viz., 0.43 vs 0.116 mdyn Å^{-1}, the splittings for the former are significantly smaller than for the latter, an obvious consequence of the different DDC interactions in the two structures.

As can be seen from Table III, the frequency and ir intensity agreement for Ala_3(AP) is excellent. Although A and B species modes are both ir and Raman active, the B species modes are, as expected, most intense in the ir. The most intense ir band at 1641–1647 cm^{-1} is at a higher frequency than the comparable 1632-cm^{-1} band of β-PLA, although the weaker high-frequency component at 1691 cm^{-1} is closer to its β-PLA counterpart at 1694 cm^{-1}.[6,7,19] The intense Raman band at 1658 cm^{-1} is at a lower frequency than the related band at 1669 cm^{-1} in β-PLA.[6,7,19] These differences are a reflection of the different structures involved.

For Ala_3(P), we see from Table IV that the pattern of observed frequencies is, as expected, different from that in Ala_3(AP), and these differences are very well reproduced by the calculation. The intense Raman and ir bands, at 1662 and 1649 cm^{-1}, respectively, are similar to comparable bands at 1657 and 1645 cm^{-1} in parallel-chain L-Val-Gly-Gly,[12] and interestingly close to those at 1663 and 1642 cm^{-1}, predicted for an infinite parallel-chain β-sheet PLA.[20]

The predicted downshifts on N-deuteration are in the range of 3–5 cm^{-1}, which corresponds well with observation.

Table II End Group Force Constants of Ala_3[a]

	Ala_3		
	AP	P	L-Val-Gly-Gly
NH_3^+			
NC^α	4.523		4.823
NH	5.163		
$NC^\alpha H^\alpha$	0.715		0.765
$NC^\alpha C$	0.819		
$C^\alpha NH$	0.829		
HNH	0.560	0.539	0.549
NC^α t	0.366		0.250
NH t	0.0005		
NH, NH	0.022		
NC^α, $C^\alpha C$	0.300		
NC^α, $C^\alpha NH$	0.294		
NC^α, HNH	−0.150		
NC^α, $NC^\alpha C$	0.300		0.600
NC^α, $NC^\alpha H^\alpha$	0.627		
$C^\alpha C$, $NC^\alpha C$	0.300		
$C^\alpha C^\beta$, $NC^\alpha H^\alpha$	0.079		
$NC^\alpha C$, $NC^\alpha C^\beta$	0.200		0.150
$NC^\alpha H$, $C^\alpha NH$	0.010		
$NC^\alpha C$, $CC^\alpha C^\beta$	−0.041		−0.141
$C^\alpha NH$, $C^\alpha NH$	−0.087	−0.040	−0.040
HNH, HNH	0.007	−0.0149	−0.015
CO_2^-			
CO	9.400		9.500
OCO	2.100		
$C^\alpha CO$	0.511		1.109
$C^\alpha C$ t	0.155		
CO t	0.001		
CO, CO	1.300	1.400	1.400
CO, $C^\alpha C$	0.9584		
CO, OCO	0.0		−0.135
CO, $C^\alpha CO$	0.889		0.700
$C^\alpha C$, $C^\alpha CO$	0.300		
$C^\alpha C$, OCO	−0.547		−0.652
$C^\alpha CO$, $C^\alpha CO$	0.0	−0.100	−0.100
CO_2 wag	0.542		0.577
CO_a, $C^\alpha CO_b$	−0.509		
CO_2 w, $CC^\alpha H^1$	0.0		−0.093
CO_2 w, $CC^\alpha H^2$	0.0		0.093

[a] A blank space means that the force constant is the same as the previous one.

Amide II. Since we have not altered force constants associated with NH in-plane bend (ib) to mirror differences in hydrogen-bond strengths, which would be justifiable,[14] the present calculations reflect mainly the effects of DDC on amide II frequencies. The results are, nevertheless reasonable.

For Ala_3(AP), the unperturbed frequencies of the intense ir modes are 1543 and 1536 cm^{-1}; DDC shifts these to 1558 and 1531 cm^{-1}, compared to observed bands at 1547 and 1536 cm^{-1}. In β-PLA the observed (and calculated) ir bands are at 1555 (1562) and 1524 (1528) cm^{-1}.[6,7,19] For Ala_3(P), the unperturbed strong ir mode is at 1535 cm^{-1}, with DDC shifting it only slightly (to 1536 cm^{-1}), compared to the observed band at 1525 cm^{-1}. In L-Val-Gly-Gly, the comparable calculated frequencies are 1538 and 1541 cm^{-1}, with the observed strong band being at 1543 cm^{-1}. It is clear that, while the general features of amide II in Ala_3 can be accounted for, improvement in specific details will require further refinements in the force field.

On N-deuteration, amide II′ for Ala_3(AP) is predicted at 1479 and 1477 cm^{-1} (for A and B species), with observed bands being seen at 1487M(R), 1479M(ir), and 1473W(R) cm^{-1}. For Ala_3(P), the predicted amide II′ frequencies are 1479, 1478, 1477, and 1474 cm^{-1}, and bands are observed at 1485M(R), 1475W(R), and 1470MS(ir) cm^{-1}.

Amide III. As has been discussed in detail,[4] the so-called amide III is a complex mode that has been thought to be characterized by NH ib + CN s contributions, but whose detailed nature is in fact sensitively dependent on the specifics of backbone-chain conformation and side-chain composition. In β-PLA[6,7,19] CN s does contribute significantly; in Ala_3 this contribution is variable.

If we consider all modes in the $\sim$ 1400–1170-cm^{-1} region that contain NH ib, and therefore should be sensitive to N-deuteration, then agreement between calculated and observed frequencies is reasonably good. For Ala_3(AP), with observed deuteration-sensitive bands in brackets, modes with NH ib are predicted at the following: 1350, 1348 [1353]; 1270, 1264 [1267]; 1263 [1247]; 1258 [1242]; 1234, with C_2N sA(7) [1232]; 1196 [1206?]; 1193; and 1176, with C_1N sB(6). The situation is complicated somewhat by the contributions of NH_3^+ rock (r) in this region, but the agreement is generally satisfactory. For Ala_3(P), the corresponding bands are at the following; 1354, 1353 [1344]; 1283, with C_1N sA(9), and 1271, with C_1N sB(8) [1279?]; 1266, with C_2N sA(5); 1259, with C_2N sB(5) [1252]; and 1191. Again, NH_3^+ r contributions overlap these modes, making definitive identifications difficult. However, if the calculated modes are correct (in the context that we have not adjusted force constants for NH ib), then we see, for example, that it would be inappropriate to associate the 1226MS cm^{-1} Raman band of Ala_3(P), which is attributable to NH_3^+ r, to the same kind of mode as the 1229MS cm^{-1} Raman band of Ala_3(AP), which is assignable to NH ib. Thus, Ala_3(P) does not seem to exhibit the usual Raman bands associated with amide III.

On N-deuteration, the corresponding ND ib modes are predicted to contribute primarily to bands at 997, 996, 986, 983, 933, and 929 cm^{-1} for Ala_3(AP), and new observed bands at 1003MS(R), 998M(ir), 947W(R), 942W(ir), and 936MS(ir), 931MS(R) cm^{-1} may be assignable to these modes. The problem is that ND_3^+ r modes are also expected in this region, at 971, 966, 948, and 942 cm^{-1}, and exact assignments cannot be made at this time. For Ala_3(P) ND ib is predicted to contribute primarily to bands at 998, 997, 996, 988, 922, and 913 cm^{-1}, with ND_3^+ r contributing primarily at 956, 953, and 942 cm^{-1}. New bands are found at 1003MS(R), 991MS(ir), 946VW(R), 941W(ir), 933MS(R), and 927M(ir), that are undoubtedly assignable to these modes, although a detailed correspondence may be difficult at this time. Despite this, it is clear that the general deuteration shifts are reasonably well accounted for.

Amide V. The amide V mode, essentially NH out-of-plane bend (ob) plus CN torsion (t), should be very sensitive to hydrogen-bond strength for a given side-chain composition and main-chain conformation,[4] and we may therefore expect significant differences between Ala_3(AP) and Ala_3(P). This is the case, and the normal mode calculations predict the frequencies quite well.

For Ala_3(AP), major predicted and deuteration-sensitive (in brackets) observed frequencies are located at the following: 725 [725]; 692 [696]; 690 [687]; and 683 [676] cm^{-1}. For Ala_3(P), the comparable modes are at the following: 701 [701]; 690 [682]; 666 [653]; 656 [642]; 643 [631]; 633 [626]; 625 [618]; and 608 [605] cm^{-1}. As can be seen, the internal coordinates of amide V can contribute quite differently to normal modes in this region depending on the structure. The higher frequency range for Ala_3(AP), 725–683 cm^{-1}, than for Ala_3(P), 701–608 cm^{-1}, is consistent with the stronger interpeptide hydrogen bonds in the former than in the latter.

The ND ob coordinate in Ala_3(AP) is predicted to contribute to modes at 528, (517), (513), 510, 502, 490, and (475) cm^{-1} (the parentheses indicate

Table III Observed and Calculated Frequencies (in cm^{-1}) of Ala_3(AP)

Observed[a]		Calculated		
Raman	ir	A	B	Potential Energy Distribution[b]
	1691MW		1686[c]	C_1O sA(73) C_1N sA(19) [7.9]
		1681[c]		C_1O sA(73) C_1N sA(19) [0.3]
	1667sh		1666[c]	C_2O sA(59) C_2N sA(18) C_2O sB(12) [3.2]
1667sh		1665[c]		C_2O sA(59) C_2N sA(18) C_2O sB(12) [0.4]
1658S		1657[c]		C_2O sB(50) C_2N sB(15) C_2O sA(11) C_1O sB(11) [0.1]
1639sh		1645[c]		C_1O sB(62) C_2N sB(15) C_2O sB(11) [0.7]
	1647sh		1645[c]	C_2O sB(50) C_2N sB(15) C_2O sA(11) C_1O sB(11) [10.7]
	1641VS		1643[c]	C_1O sB(62) C_1N sB(15) C_2O sB(11) [14.3]
	1623W	1636	1636	N_1 ab2B(69) N_1 r1B(18)
		1630	1630	N_1 ab1A(35) N_1 ab2A(35) N_1 r2A(22)
1613VW		1608	1608	N_1 ab1B(72) N_1 r2B(19)
		1607	1607	N_1 ab2A(38) N_1 ab1A(37) N_1 r1A(20)
	1595W	1597	1597	O_2 asB(105)
		1596	1596	O_2 asA(106)
		1571[c]		N_3H ibA(42) C_2N sA(17) $C_2^{\alpha}C$ sA(12) [1.5]
			1567[c]	N_3H ibA(41) C_2N sA(16) $C_2^{\alpha}C$ sA(12) [1.4]
		1567[c]		N_3H ibB(40) C_2N sB(16) $C_2^{\alpha}C$ sB(12) N_2H ibB(6) [0.2]
	1547S		1558[c]	N_3H ibB(39) C_2N sB(16) $C_2^{\alpha}C$ sB(12) N_2H ibB(6) [7.5]
1551W		1557[c]		N_2H ibB(23) N_1 sbB(17) C_1N sB(12) N_3H ibB(7) [0.0]
1536W		1533[c]		N_2H ibA(27) N_1 sbA(14) C_1N sA(13) [0.3]
			1531[c]	N_2H ibB(22) N_1 sbB(16) C_1N sB(11) N_3H ibB(7) N_2H ibA(6) [15.4]
	1536S			
			1531[c]	N_2H ibA(26) N_1 sbA(14) C_1N sA(13) N_2H ibB(6) [1.3]
	1508sh	1517	1517	N_1 sbB(69) N_2H ibB(12)
		1515	1515	N_1 sbA(73) N_2H ibA(10)
		1455	1455	C_2H_3 ab2B(38) C_1H_3 ab2B(22) C_3H_3 ab2B(18)
		1455	1455	C_2H_3 ab2A(39) C_1H_3 ab2A(20) C_3H_3 ab2A(20)
		1453	1453	C_3H_3 ab2B(37) C_1H_3 ab2B(26)
		1453	1453	C_3H_3 ab2A(37) C_1H_3 ab2A(27)
1471sh		1452	1452	C_2H_3 ab1B(19) C_2H_3 ab2B(18) C_3H_3 ab2B(14) C_3H_3 ab1B(12)
1457MS	1459MS	1452	1452	C_2H_3 ab1A(21) C_2H_3 ab2A(18) C_3H_3 ab2A(12) C_3H_3 ab1A(11)
	1447W	1452	1452	C_3H_3 ab1A(29) C_2H_3 ab1A(23) C_1H_3 ab2A(11)
	1443VW	1452	1452	C_3H_3 ab1B(25) C_2H_3 ab1B(23) C_1H_3 ab2B(12)
		1452		C_1H_3 ab1B(42) C_1H_3 ab1A(21) C_3H_3 ab1B(13)
			1452	C_1H_3 ab1A(63) C_3H_3 ab1A(16)
		1452		C_1H_3 ab1A(45) C_1H_3 ab1B(21) C_3H_3 ab1A(11)
			1452	C_1H_3 ab1B(60) C_3H_3 ab1B(19)
		1451	1451	C_2H_3 ab1A(17) C_2H_3 ab2A(15) C_2H_3 ab2B(14) C_3H_3 ab1B(12)
		1451	1451	C_2H_3 ab1B(18) C_2H_3 ab2B(15) C_3H_3 ab1B(12) C_1H_3 ab1B(11)
		1411	1411	O_2 ssB(55) O_2 bB(25) $C_3^{\alpha}C$ sB(11)
1409MW	1411S	1410	1410	O_2 ssA(56) O_2 bA(25) $C_3^{\alpha}C$ sA(12)
		1402	1402	C_1H_3 sbB(16) H_2 b2B(12) N_2H ibB(5)
1396W	1400sh	1400	1400	C_1H_3 sbA(17) H_2 b2A(12) N_2H ibA(6)
		1388	1388	C_1H_3 sbB(25) C_2H_3 sbB(22)
		1387	1387	C_2H_3 sbA(26) C_1H_3 sbA(21)
1379W	1377MW	1382	1382	C_3H_3 sbA(67) H_3 b1A(13) C_2H_3 sbA(10)
		1382	1382	C_3H_3 sbB(68) H_3 b1B(13)
		1373	1373	C_2H_3 sbB(43) C_1H_3 sbB(13) H_2 b2B(11)
1363MW	1364MS	1372	1372	C_2H_3 sbA(37) C_1H_3 sbA(19) H_2 b2A(11)

Table III *(Continued from the previous page.)*

Observed[a]		Calculated		
Raman	ir	A	B	Potential Energy Distribution[b]
1353VW	1352VW	1350	1350	H_3 b2A(22) C_1H_3 sbA(20) H_1 b2A(11) N_2H ibA(9)
		1348	1348	H_3 b2B(25) C_1H_3 sbB(18) H_1 b2B(10) N_2H ibB(8)
1330sh	1331W	1322	1322	N_1 r2B(31) N_1 ab2B(13) N_1 r1B(12)
1323W	1323W	1315	1315	H_2 b2A(22) N_1 r2A(20) H_3 b2A(16)
1307MW	1306W	1308	1308	H_1 b2B(29) H_2 b2B(22) H_3 b2B(13)
		1296	1296	H_1 b2A(26) N_1 r1A(23) N_1 r2A(12) N_1 ab2A(10)
1266MS	1268M	1270	1270	N_1 r1B(27) N_2H ibB(11)
		1264	1264	NC_2^{α} sA(16) N_2H ibA(7)
1247MW	1248sh	1263	1263	N_1 r1A(19) N_2H ibA(7)
		1263	1263	N_1 r1A(18)
	1242sh	1258	1258	N_3H ibB(17) H_3 b2B(16) H_1 b2B(12)
1229MS	1234MS	1234	1234	N_3H ibA(22) H_3 b2A(18)
	1221VW	1210	1210	NC_3^{α} sA(24) $C_3^{\alpha}C^{\beta}$ sA(24) H_3 b1A(11)
	1206VW	1207	1207	NC_3^{α} sB(22) $C_3^{\alpha}C^{\beta}$ sB(21) H_2 b1B(12)
		1196	1196	NC_1^{α} sB(20) H_1 b2B(11) N_2H ibB(11)
		1193	1193	H_1 b2A(14) N_2H ibA(14) NC_1^{α} sA(10) H_2 b2A(10)
1169sh		1179	1179	NC_1^{α} sA(25) $C_1^{\alpha}C^{\beta}$ sA(14) N_1 r2A(9)
		1176	1176	NC_1^{α} sB(15) $C_1^{\alpha}C^{\beta}$ sB(10) $C_2^{\alpha}C^{\beta}$ sB(10) N_2H ibB(6)
1159MW	1158MW	1171	1171	H_3 b1B(41) C_3H_3 sbB(16) C_3H_3 r1B(10)
		1170	1170	H_3 b1A(43) C_3H_3 sbA(17) C_3H_3 r1A(11)
1146sh	1148MS	1139	1139	H_2 b1A(40) C_2H_3 sbA(14) C_2H_3 r1A(12)
		1137	1137	H_2 b1B(40) C_2H_3 sbB(14) C_2H_3 r1B(12)
1120VW	1122W	1124	1124	H_1 b1A(61) C_1H_3 sbA(20)
1108MW	1110W	1120	1120	H_1 b1B(58) C_1H_3 sbB(20) C_1H_3 r2B(11)
	1090VW	1089	1089	C_2H_3 r2A(26) $C_2^{\alpha}C^{\beta}$ sA(20) C_3H_3 r2A(13) C_3H_3 r1A(11)
		1087	1087	C_2H_3 r2B(32) $C_2^{\alpha}C^{\beta}$ sB(23)
1082S	1083VW	1083	1083	C_3H_3 r2A(34) $C_3^{\alpha}C^{\beta}$ sA(15) C_2H_3 r2A(13)
		1083	1083	C_3H_3 r2B(39) $C_3^{\alpha}C^{\beta}$ sB(20) C_2H_3 r2B(10)
1077sh	1077sh	1066	1066	$C_3^{\alpha}C^{\beta}$ sA(22) C_3H_3 r1A(20) H_3 b1A(17)
1067VW		1064	1064	C_1H_3 r1A(28) C_1H_3 r2A(19) H_1 b1A(10)
		1064	1064	C_1H_3 r1B(35)
1054MW	1055MS	1063	1063	C_2H_3 r1B(16) C_3H_3 r1B(12) H_2 b1B(10) C_1H_3 r1B(10)
		1061	1061	C_2H_3 r1A(35) H_2 b1A(13) $C_2^{\alpha}C^{\beta}$ sA(11)
	1050sh	1059	1059	C_2H_3 r1B(22) C_3H_3 r1B(13) H_3 b1B(11) $C_2^{\alpha}C^{\beta}$ sB(10) $C_3^{\alpha}C^{\beta}$ sB(10)
1018W	1016M	1051	1051	$C_1^{\alpha}C^{\beta}$ sA(39) C_1H_3 r2A(17) C_1H_3 r1A(12) N_1 r2A(5)
		1046	1046	$C_1^{\alpha}C^{\beta}$ sB(39) C_1H_3 r2B(28) N_1 r2B(7)
	967S	964	964	C_2H_3 r2A(16) NC_2^{α} sA(12)
960MW	961sh	963	963	C_2H_3 r2B(15) NC_2^{α} sB(12)
944VW	949W	944	944	NC_3^{α} sA(12) C_3H_3 r2A(10)
		942	942	NC_3^{α} sB(13)
920sh	924MW	923	923	NC_1^{α} sA(14)
	918sh	919	919	NC_1^{α} sB(13)
902VS	900MW	905	905	C_2N sA(10)
		900	900	C_2N sB(10)
	882W	880	880	$C_3^{\alpha}C$ sA(18) O_2 bA(12)
876VW	875VW	876	876	$C_3^{\alpha}C$ sB(19) O_2 bB(15) O_2 ssB(11)
861MW	861MW	847	847	$C_1^{\alpha}C$ sA(9) O_2 bA(9)
	848W	844	844	NC_1^{α} sB(11) $C_1^{\alpha}C$ sB(10)
789VW	790W	778	778	C_2O obA(38)

Table III *(Continued from the previous page.)*

Observed[a]		Calculated		
Raman	ir	A	B	Potential Energy Distribution[b]
	774MW	774	774	C_2O obB(43)
		768	768	C_1O obA(32)
769sh		766	766	C_1O obB(36)
		763	763	O_2 wA(16) O_2 bA(13) C_1O obA(11)
760W	761sh	759	759	O_2 wB(23) O_2 bB(12) C_1O obB(12)
725W	725W	725	725	C_2N tA(60) N_3H obA(33)
		714	713	C_2N tB(15) O_2 wB(11)
		703	703	$C_1^{\alpha}C$ sA(10) C_1N tA(10) N_3H obA(7)
695VW	696VS	692	692	C_1N tA(64) N_2H obA(36)
	687W	690	690	C_2N tB(50) N_3H obB(30) C_1N tB(10)
677W	675VW	683	683	C_1N tB(64) N_2H obB(33)
			661	O_2 bB(10)
654VW	655MS	660		O_2 bB(13) C_1O ibB(10) $C_3^{\alpha}C$ sB(10) N_2H obB(6)
		658	657	O_2 wA(13) C_1O ibA(12) O_2 bA(11)
		637	637	C_2O ibA(17) C_1O ibA(13)
633W	632MS	633	632	C_2O ibB(18) C_1O ibB(17)
		577	577	O_2 rB(13) $NC_3^{\alpha}C$ dB(11)
592VW	593W	570	570	O_2 rA(16)
		532	531	NC_1^{α} tB(54) N_1H tB(12)
		518	517	H · · · O s11(43) H · · · O s12(38)
		516	517	H · · · O s11(44) H · · · O s12(44)
		510	510	NC_1^{α} tA(65)
		505	505	$NC_3^{\alpha}C$ dB(20) H · · · O s12(14) C_3^{β} b2B(11) N_3H obB(7)
489VW	490VW	489	489	$NC_3^{\alpha}C$ dA(22) C_3^{β} b2(16) N_3H obA(6)
		454	454	C_1^{β} b2B(32) C_2^{β} b2B(14)
458W	462MS	451	451	C_1^{β} b2A(25) C_2^{β} b2A(20)
436MW		421	421	C_3^{β} b1A(19) C_2^{β} b1A(14) N_3H obA(8)
396VW		413	413	C_2^{β} b1B(15) N_2H obB(7)
		352	353	O_2 rB(10) C_3^{β} b2B(10)
345VW		349	348	C_1^{β} b1A(9) C_3^{β} b1A(9) $C_1^{\alpha}CN$ dA(9) O_2 rA(9)
325VW		318	318	C_3^{β} b2B(20) O_2 wB(13) C_2O ibB(10)
306MW		303	303	$NC_2^{\alpha}C$ dA(14) $NC_3^{\alpha}C$ dA(12) O_2 wA(12) C_2^{β} b2A(12)
		300	299	C_3^{β} b2A(27) C_2O ibA(15) O_2 wA(13) $NC_3^{\alpha}C$ dA(10) CNC_3^{α} dA(10)
293sh		296	294	C_1^{β} b2A(21) $NC_1^{\alpha}C$ dA(18) C_1^{β} b1A(15) C_1O ibA(13)
		290	290	C_1^{β} b2B(22) C_1^{β} b1B(19) C_1O ibB(17) $NC_1^{\alpha}C$ dB(16)
		285	285	C_2^{β} b2B(12) C_3^{β} b1B(12) $NC_2^{\alpha}C$ dB(10) C_2O obB(10)
269VW		265	264	O_2 rB(15) $C_3^{\alpha}C^{\beta}$ t(13) $C_2^{\alpha}C^{\beta}$ t(11)
		255	255	$C_2^{\alpha}C^{\beta}$ tA(23) C_2^{β} b2A(12) $C_3^{\alpha}C^{\beta}$ tA(11)
		251		$C_1^{\alpha}C^{\beta}$ tA(36) $C_1^{\alpha}C^{\beta}$ tB(15)
251sh			250	$C_1^{\alpha}C^{\beta}$ tA(43) C_1O obA(10)
		249	249	$C_1^{\alpha}C^{\beta}$ tB(54)
		241		$C_2^{\alpha}C^{\beta}$ tB(32) $C_3^{\alpha}C^{\beta}$ tA(23) $C_3^{\alpha}C^{\beta}$ tB(22)
242M			241	$C_2^{\alpha}C^{\beta}$ tB(53) $C_3^{\alpha}C^{\beta}$ tB(28)
			241	$C_3^{\alpha}C^{\beta}$ tA(61) $C_2^{\alpha}C^{\beta}$ tA(22)
		241		$C_3^{\alpha}C^{\beta}$ tA(40) $C_2^{\alpha}C^{\beta}$ tB(19) $C_2^{\alpha}C^{\beta}$ tA(17)
		236		$C_1^{\alpha}C^{\beta}$ tA(23) $C_2^{\alpha}C^{\beta}$ tA(22) $C_3^{\alpha}C^{\beta}$ tB(10)
			236	$C_2^{\alpha}C^{\beta}$ tA(28) $C_3^{\alpha}C^{\beta}$ tB(17)
		233		$C_3^{\alpha}C^{\beta}$ tB(23) $C_2^{\alpha}C^{\beta}$ tA(21) O_2 rB(10)

Table III *(Continued from the previous page.)*

Observed[a]		Calculated		
Raman	ir	A	B	Potential Energy Distribution[b]
			233	$C_3^{\alpha}C^{\beta}$ tB(18) $C_2^{\alpha}C^{\beta}$ tB(14) $C_2^{\alpha}C^{\beta}$ tA(11) O_2 rB(10)
		229	229	C_2^{β} b2B(14)
		224	223	O_2 rA(31)
226VW			222	$C_1^{\alpha}C^{\beta}$ tA(19) $C_1^{\alpha}CN$ dA(10)
		221		C_1^{β} b1A(8) C_3^{β} b2A(8)
		213	215	C_1^{β} b1B(14)

[a] S, strong; M, medium; W, weak; V, very; sh, shoulder.

[b] s, Stretch; ss, symmetric stretch; as, antisymmetric stretch; b, bend; sb, symmetric bend; ab, antisymmetric bend; ib, in-plane bend; ob, out-of-plane bend; d, deformation; w, wag; r, rock; t, torsion; N_1, NH_3^+; O_2, CO_2^-. Only contributions of 10 or greater are included, except for NH and NH_3^+, for which contributions of 5 or greater are included.

[c] Includes DDC interactions.

smaller contributions); new bands are observed in the ir on N-deuteration at 523 and 505 cm^{-1}, which can be assigned to such modes. For Ala_3(P), ND ob is predicted in modes at (575), (516), (511), 488, (457), 452, and (434) cm^{-1}; new ir bands are observed at 572, 518, 513, 475, and 463 cm^{-1}, again in reasonable agreement with the calculations.

End-Group Modes

The nonstretching modes of the NH_3^+ and CO_2^- end groups are well predicted by the calculations, and the frequencies are consistent with values found for L-Val-Gly-Gly[12] and Gly_3.[16] We note, however, some special features of these modes in Ala_3.

The 1593VS cm^{-1} ir band of Ala_3(P) and the 1595MW cm^{-1} ir band of Ala_3(AP) are clearly assignable to CO_2^- antisymmetric stretch (as) since they are hardly affected by N-deuteration. It may seem strange that the intensities of these bands are so different in the two structures, but apparently the intensity of this mode is very sensitive to the environment. For example, in L-Val-Gly-Gly and Gly_3 we found this mode to be weak in the parent molecules but much more intense in the N-deuterated molecules. In Ala_3 there is not much intensity change on deuteration, but the initial intensities are significantly different. This is not true of CO_2^- symmetric stretch (ss), which is equally strong for both structures.

The frequency ranges over which NH_3^+ r makes its main contribution are significantly different in these molecules: 1207–1155 cm^{-1} in Gly_3, 1208 cm^{-1} in L-Val-Gly-Gly, 1322–1263 cm^{-1} in Ala_3(AP), and 1267–1238 cm^{-1} in Ala_3(P). It is not clear what these differences arise from, but they may be related to the different hydrogen-bonding environments (there seems to be no correlation with similarities or differences in end-group side chain).

The CO_2^- r mode is predicted at ~ 585–570 cm^{-1} for Gly_3, L-Val-Gly-Gly, and Ala_3(AP), but much lower, 427 and 355 cm^{-1}, for Ala_3(P). The reason is not obvious.

CH_3 and Skeletal Modes

The assignments of CH_3 and skeletal modes are clear in some cases but must be considered tentative in others, particularly since this part of the force field has been transferred without change from β-PLA.[6,7] The major features of these assignments are, however, certainly delineated by the relatively large frequency gaps in certain regions (e.g., the ~ 67-cm^{-1} gap centered near 810–820 cm^{-1} and the ~ 80-cm^{-1} gap centered near 1004 cm^{-1}).

The observed bands in the ~ 1460–1440 region are clearly assignable to CH_3 antisymmetric bend (ab), as are the bands in the ~ 1400–1370-cm^{-1} region to CH_3 symmetric bend (sb). The specific assignments to modes are reasonable if not certain. From about 1200 cm^{-1}, NC^{α}s, $C^{\alpha}C^{\beta}$s, and H^{α} bend (b) begin to contribute, mixing differently (and with some NH ib, CH_3 sb, and CH_3 r) for the two structures. We think the proposed assignments are reasonable, although the frequency agreement is occasionally poor. A glaring example involves $C_1^{\alpha}C^{\beta}$ s [cf. the calculated modes at 1051 and 1046 cm^{-1} in Ala_3(AP) with the clearly assignable observed bands, and the similar ones at 1046 and 1043 cm^{-1} in Ala_3(P)], and may indicate that this terminal force constant may need to be modified. Below this frequency gap and down to the amide V modes the

Table IV Observed and Calculated Frequencies (in cm^{-1}) of $Ala_3(P)$

Observed[a]		Calculated		
Raman	ir	A	B	Potential Energy Distribution[b]
	1686sh		1683[c]	C_1O sA(77) C_1N sA(19) [7.8]
		1673[c]		C_1O sA(77) C_1N sA(18) [0.2]
	1668W		1665[c]	C_2O sA(76) C_2N sA(18) [8.3]
1662S		1663[c]		C_2O sA(76) C_2N sA(18) [0.2]
			1655[c]	C_2O sB(62) C_2N sB(18) [6.3]
	1649VS		1654[c]	C_1O sB(60) C_1N sB(18) [13.1]
		1651[c]		C_2O sB(62) C_2N sB(18) [0.5]
1648sh		1651[c]		C_1O sB(60) C_1N sB(18) C_2O sB(10) [0.0]
		1630	1630	N_1 ab1A(53) N_1 ab2A(22) N_1 r2A(17)
1630VW	1628VW	1629	1629	N_1 ab2B(55) N_1 ab1B(19) N_1 r2B(12)
		1609	1609	N_1 ab1B(61) N_1 ab2B(19) N_1 r1B(13)
		1592	1592	O_2 asB(84) N_1 ab2A(12)
	1593VS	1591	1591	N_1 ab2A(44) O_2 asB(23) N_1 ab1A(18) N_1 r1A(12)
		1590	1590	O_2 asA(103)
		1567[c]		N_2H ibB(40) C_1N sB(15) $C_1^{\alpha}C$ sB(10) [0.3]
1568W		1562[c]		N_2H ibA(41) C_1N sA(18) $C_1^{\alpha}C$ sA(10) N_1 sbA(8) [0.9]
			1561[c]	N_2H ibB(40) C_1N sB(15) $C_1^{\alpha}C$ sB(10) [2.0]
	1550sh		1549[c]	N_2H ibA(40) C_1N sA(18) $C_1^{\alpha}C$ sA(10) N_1 sbA(7) [2.5]
	1525S		1536[c]	N_3H ibB(31) C_2N sB(13) N_3H ibA(13) [17.9]
			1529[c]	N_3H ibA(33) C_2N sA(14) N_3H ibB(11) [1.4]
		1529[c]		N_3H ibB(32) C_2N sB(13) N_3H ibA(12) [0.5]
1522W		1520[c]		N_3H ibA(34) C_2N sA(15) N_3H ibB(10) [0.2]
		1520	1520	N_1 sbB(85)
	1506sh	1514	1514	N_1 sbA(84) N_2H ibA(7)
		1455	1455	C_1H_3 ab2B(36) C_2H_3 ab2B(30) C_3H_3 ab1B(12)
		1454	1454	C_2H_3 ab1A(32) C_1H_3 ab2A(23) C_3H_3 ab1A(18)
		1453	1453	C_1H_3 ab2A(41) C_3H_3 ab1A(26) C_3H_3 ab2A(14)
		1453	1453	C_3H_3 ab1B(37) C_1H_3 ab2B(24) C_3H_3 ab2B(14)
1470sh		1453	1453	C_2H_3 ab2A(37) C_3H_3 ab2A(30)
1454MS	1451MS	1453	1453	C_3H_3 ab2B(42) C_2H_3 ab2B(24) C_2H_3 ab1B(16)
	1422sh	1452	1452	C_3H_3 ab2A(35) C_2H_3 ab2A(26) C_3H_3 ab1A(18)
		1452	1452	C_3H_3 ab2B(28) C_2H_3 ab1B(26) C_3H_3 ab1B(21)
		1452	1452	C_2H_3 ab1A(34) C_3H_3 ab1A(16) C_1H_3 ab1A(14)
		1452	1452	C_1H_3 ab1B(63)
		1452	1452	C_1H_3 ab1A(72)
		1451	1451	C_2H_3 ab1B(32) C_1H_3 ab1B(22) C_2H_3 ab2B(15) C_1H_3 ab2B(10)
		1411	1411	O_2 ssB(52) O_2 bB(22)
1412M	1407S	1410	1410	O_2 ssA(56) O_2 bA(24) $C_3^{\alpha}C$ sA(10)
		1405	1405	H_2 b2A(15) O_2 ssA(12) N_2H ibA(6)
1394VW	1393sh	1404	1404	C_1H_3 sbB(14) O_2 ssB(14) H_2 b2B(10) N_2H ibB(6)

Table IV (*Continued from the previous page.*)

Observed[a]		Calculated		
Raman	ir	A	B	Potential Energy Distribution[b]
		1389	1389	C_1H_3 sbA(35) C_2H_3 sbA(11)
		1388	1388	C_3H_3 sbB(20) C_1H_3 sbB(17) C_2H_3 sbB(15)
		1381	1381	C_3H_3 sbA(59) C_2H_3 sbA(14) H_3 b1A(11)
1382sh	1382W	1381	1381	C_3H_3 sbB(41) C_2H_3 sbB(36)
		1372	1372	C_1H_3 sbB(27) C_2H_3 sbB(24) H_2 b2B(11) C_3H_3 sbB(10)
1364W	1363M			
		1370	1370	C_2H_3 sbA(48) H_2 b2A(12) C_1H_3 sbA(10)
	1355W	1354	1354	H_3 b2B(26) C_1H_3 sbB(17) N_2H ibB(5)
1347W	1344W	1353	1353	H_3 b2A(26) C_1H_3 sbA(16) N_2H ibA(7)
1324MW	1326MW	1332	1332	H_2 b2A(29) H_1 b2A(19) H_3 b2A(14) C_1H_3 sbA(10) N_1 r2A(7)
1313MW	1308W	1321	1321	H_2 b2B(30) H_3 b2B(16) H_1 b2B(14) N_1 r2B(10)
		1283	1283	NC_2^{α} sA(20) N_2H ibA(11) $C_2^{\alpha}C^{\beta}$ sA(10) H_1 b2A(10)
1278M	1279M			
		1271	1271	NC_2^{α} sB(24) N_2H ibB(13) $C_2^{\alpha}C^{\beta}$ sB(11)
		1267	1267	N_1 r1B(23) $C_1^{\alpha}C^{\beta}$ sB(19) H_1 b2B(18) N_1 r2B(13) N_1 ab2B(7)
		1266	1266	H_3 b2A(29) N_3H ibA(14) NC_3^{α} sA(12) N_1 r2A(5)
		1265	1265	N_1 r2A(22) H_1 b2A(19) $C_1^{\alpha}C^{\beta}$ sA(18) N_1 r1A(7) N_1 ab1A(7)
1250W	1253VW	1259	1259	H_3 b2B(28) N_3H ibB(19) N_1 r1B(6)
1226MS		1247	1247	N_1 r1B(35) N_1 r2B(23) N_1 ab1B(10)
1211sh	1214W	1238	1238	N_1 r1A(60) N_1 ab2A(12) N_1 r2A(7)
	1204MS	1199	1199	NC_3^{α} sB(22) $C_3^{\alpha}C^{\beta}$ sB(18) H_2 b1B(16)
		1198	1198	NC_3^{α} sA(12) H_1 b2A(11)
		1191	1191	H_1 b2B(15) NC_2^{α} sB(12) N_2H ibB(12)
		1191	1191	H_2 b1A(13) $C_2^{\alpha}C^{\beta}$ sA(10)
		1175	1175	NC_1^{α} sB(26) N_1 r2B(12) C_1H_3 r2B(10) $C_1^{\alpha}C^{\beta}$ sB(10)
1167sh	1165W	1169	1169	H_2 b1A(18) NC_1^{α} sA(15) N_1 r2A(8)
1158W	1154M	1160	1160	H_3 b1B(53) C_3H_3 sbB(17)
		1157	1157	H_3 b1A(48) C_3H_3 sbA(15)
1138sh	1136sh	1136	1136	H_1 b1A(31) H_2 b1A(19) C_1H_3 sbA(10)
	1128M	1130	1130	H_2 b1B(28) C_3H_3 r2B(12) C_2H_3 sbB(10)
1122MW	1120sh	1126	1126	H_1 b1B(54) C_1H_3 sbB(18)
1106VW	1107W	1117	1117	H_1 b1A(29) H_2 b1A(10) C_1H_3 sbA(10)
	1084sh	1090	1090	C_3H_3 r1B(42) C_2H_3 r2B(15) $C_2^{\alpha}C^{\beta}$ sB(11)
		1090	1090	C_3H_3 r1A(32) C_2H_3 r1A(31)
		1086	1086	C_3H_3 r1A(35) C_2H_3 r1A(28)
1080VS	1081MW	1083	1083	C_3H_3 r1B(23) C_2H_3 r2B(22) $C_3^{\alpha}C^{\beta}$ sB(13) $C_2^{\alpha}C^{\beta}$ sB(12)
		1076	1076	$C_3^{\alpha}C^{\beta}$ sA(22) $C_2^{\alpha}C^{\beta}$ sA(18) C_3H_3 r2A(15) H_3 b1A(10)
		1072	1072	$C_3^{\alpha}C^{\beta}$ sB(28) H_3 b1B(17) C_3H_3 r2B(14)
	1062M	1067	1067	C_2H_3 r2A(27) $C_2^{\alpha}C^{\beta}$ sA(21) $C_3^{\alpha}C^{\beta}$ sA(15)
1060VW		1063	1063	C_1H_3 r1B(35) C_1H_3 r2B(22) H_1 b1B(11)
	1058M	1061	1061	C_2H_3 r1B(34) H_2 b1B(13) $C_2^{\alpha}C^{\beta}$ sB(12)
		1061	1061	C_1H_3 r1A(46) C_1H_3 r2A(13) H_1 b1A(12)
1020sh	1020VW	1046	1046	$C_1^{\alpha}C^{\beta}$ sB(42) C_1H_3 r2B(20) C_1H_3 r1B(11)
1000MW	998M	1043	1043	$C_1^{\alpha}C^{\beta}$ sA(38) C_1H_3 r2A(34) N_1 r1A(5)

Table IV (*Continued from the previous page.*)

Observed[a]		Calculated		
Raman	ir	A	B	Potential Energy Distribution[b]
964MW	964S	962	962	C_2H_3 r2B(18) NC_2^a sB(14)
	959sh	960	960	C_2H_3 r2A(21) NC_2^a sA(13) C_3H_3 r2A(11)
950sh	950W	940	940	NC_1^a sB(11) NC_3^a sB(11) C_3H_3 r2B(10)
		940	940	C_3H_3 r2A(13) NC_3^a sA(12)
918VW	917MW	913	913	NC_2^a sB(11) NC_1^a sB(10) C_3^aC sB(10)
		906	906	NC_1^a sA(16) NC_2^a sA(12)
898VS	900sh	901	901	C_2N sB(10)
	893W	896	896	C_2N sA(10)
879W	879W	877	877	C_3^aC sB(18) O_2 bB(13)
		876	876	C_3^aC sA(21) O_2 bA(14) O_2 ssA(10)
860MW	864sh	863	863	NC_1^a sA(20)
	857MS	853	853	NC_1^a sB(9) $C_1^aC^\beta$ sB(9)
788VW	786W	785	785	C_2O obB(34)
		784	784	C_1O obA(16) C_2O obA(13) NC_2^aC dA(11)
	774MW	774	774	C_1O obB(44) NC_1^a sB(13)
766MW	763VW	759	759	O_2 bA(26) O_2 wA(23) NC_3^aC dA(15) O_2 ssA(12)
		740	740	C_1O obA(15) O_2 bB(12)
732W	732MW	739	739	C_1O obA(14)
	718VW	723	723	O_2 wB(15) C_2O ibB(12) NC_3^aC dB(11)
702VW	700VW	701	700	C_1N tB(43) N_2H obB(25)
682VW	681MW	690	690	C_1^aC sA(21) C_1N tB(13) N_2H obB(7)
653VW	653W	665	666	C_1O ibB(18) C_2N tB(18) N_3H obB(13) C_1^aC sB(11)
	642VW	656	656	C_2N tA(51) N_3H obA(15) C_2O obA(10)
	631VS	643	643	C_2N tB(39) N_3H obB(16) C_2O ibB(11) C_1O ibB(11)
626MW	626VS	633	633	C_2N tA(29) N_3H obA(28) O_2 wA(18) C_3^aC sA(11)
	618MW	625	625	C_1N tA(83) N_2H obA(44)
606VW	604W	608	607	C_2N tB(27) O_2 wB(23) N_3H obB(19) C_3^aC sB(11)
585VW	584W	584	584	C_2O ibA(25) C_2O obA(20) C_2^aC sA(11)
		566	571	NC_1^a tB(30)
		569	567	C_1N tA(16) C_2N tA(13) N_2H obA(9)
		559	555	NC_1^a tB(23)
526W	524W	539	539	NC_1^a tA(63) $N_1H_{1a}\cdots O$ ibA(12)
		488	489	NC_3^aC dB(15) C_3^β b2B(13) O_2 wB(10) C_2N tB(10)
		485	485	C_1^β b2A(12) NC_1^aC dA(10)
		463	464	C_1^β b2B(33) NC_1^aC dB(12)
448MW	452VW	451	452	C_2O obA(12) C_2^β b2A(11) C_1O ibA(10) NC_2^aC dA(10)
		444	443	C_1^β b2A(21) C_2^aCN dA(13) NC_1^aC dA(11)
418W		427	427	O_2 rB(36) C_3^β b1B(22) O_2 wB(12)
		360	361	C_1^β b1B(15) C_1^aCN dB(14) NC_1^aC dB(10) N_2H obB(8)
		354	355	O_2 rA(40) C_3^β b1A(14) O_2 wA(11)
334W		346	346	NC_1^aC dA(16) C_1O obA(16) C_1^aCN dA(13) C_2^β b2A(10) N_2H obA(9)

Table IV *(Continued from the previous page.)*

Observed[a]		Calculated		
Raman	ir	A	B	Potential Energy Distribution[b]
316sh		308	307	C_2^β b2B(22) $NC_2^\alpha C$ dB(19)
296MW		297	300	C_1^β b1A(19) C_1^β b2A(16) $NC_1^\alpha C$ dA(11)
		296	296	C_1^β b2B(24) C_1O ibB(16) $NC_1^\alpha C$ dB(15)
		291	287	C_3^β b2A(25) O_2 wA(11) $NC_3^\alpha C$ dA(11)
		283	281	C_3^β b2B(22) $C_2^\alpha CN$ dB(18) $NC_3^\alpha C$ dB(10)
264W		270	270	CNC_2^α dB(12) C_2O ibB(11) N_3H obB(6)
244M		267	267	$C_1^\alpha C^\beta$ tA(16) $C_2^\alpha C^\beta$ tA(12)
		256	255	$C_1^\alpha C^\beta$ tB(14) O_2 rA(12)
		252	251	$C_1^\alpha C^\beta$ tB(38)
		243	243	$C_1^\alpha C^\beta$ tA(47) $C_2^\alpha C^\beta$ tA(42)
		242	241	$C_3^\alpha C^\beta$ tB(55) $C_2^\alpha C^\beta$ tB(26)
		239		$C_3^\alpha C^\beta$ tA(76)
			238	$C_3^\alpha C^\beta$ tA(51) $C_2^\alpha C^\beta$ tB(12) $C_3^\alpha C^\beta$ tB(10)
		237		$C_2^\alpha C^\beta$ tB(58) $C_3^\alpha C^\beta$ tB(23)
			237	$C_2^\alpha C^\beta$ tB(42) $C_3^\alpha C^\beta$ tB(19)
		235	234	$C_2^\alpha C^\beta$ tA(31) $C_1^\alpha C^\beta$ tA(29) C_2^β b2A(10)
		229	226	$C_1^\alpha C^\beta$ tB(26) C_1^β b1B(13)
226M		219	221	O_2 rB(29) $C_1^\alpha CN$ dB(10)
		209	209	$C_2^\alpha CN$ dA(17) C_2^β b2A(10)

[a] S, strong; M, medium; W, weak; V, very; sh, shoulder.

[b] s, Stretch; ss, symmetric stretch; as, antisymmetric stretch; b, bend; sb, symmetric bend; ab, antisymmetric bend; ib, in-plane bend; ob, out-of-plane bend; d, deformation; w, wag; r, rock; t, torsion; N_1, NH_3^+; O_2, CO_2^-. Only contributions of 10 or greater are included, except for NH and NH_3^+, for which contributions of 5 or greater are included.

[c] Includes DDC interactions.

Table V Observed Bands in the NH and CH Stretching Region (in cm^{-1})

Ala_3(AP)		Ala_3(P)		
Raman	ir	Raman	ir	Assignment
		3355S	3357VS	NH s
3342W	3342S			NH s
3318W	3318W			
3282M	3282S			NH_3^+ as
3260MW	3260MS			
3092VW				Amide B
3072W	3080M		3055MW	
3047W		3039W		NH_3^+ ss
2997MS	2999W	3009VW	3012W	CH_3 as
2978S	2980MW	2983VS	2984MW	
2965S	2966W		2968sh	
2941sh	2947MW		2946sh	CH_3 ss
2932VS	2930VW	2935VS	2935W	
2877MS	2880W	2875W	2876W	$C^\alpha H^\alpha$ s

assignments are quite secure and the frequency agreement is good. The assignments between 600 and 200 cm^{-1} must be considered suggestive at present.

NH and CH Stretch Modes

In Table V we present the observed bands in the NH s and CH s regions for Ala_3(AP) and Ala_3(P), together with general assignments that are consistent with our calculations. It is interesting to note that the NH s modes of Ala_3(AP) are definitely lower than those of Ala_3(P), consistent with its slightly stronger hydrogen bonds (although details must await a Fermi resonance analysis of the NH s + amide B bands[21]). The NH_3^+ as modes of Ala_3(P) seem not to be observed, although the NH_3^+ ss modes are seen for both structures. The CH_3 as, CH_3 ss, and $C^{\alpha}H^{\alpha}$ s modes are essentially the same for Ala_3(AP) and Ala_3(P), as might be expected.

CONCLUSIONS

Although the molecular conformations of Ala_3 are relatively similar in the two crystal structures, viz., essentially extended chains, the ir and Raman spectra of Ala_3(AP) and Ala_3(P) are distinctively different. These differences are primarily due to differences in the patterns and geometries of the hydrogen bonds in these structures, which also result in some changes in main-chain geometry (e.g., the variations in lengths of C=O bonds). Despite the limitations imposed by empirically refined vibrational force fields,[4] it has nevertheless been possible to account for these differences in significant detail by means of normal mode calculations. This indicates the essential validity of these force fields for describing the vibrational dynamics of polypeptides.

The differences between similar structures, such as Ala_3(AP) and β-PLA as well as Ala_3(P) and L-Val-Gly-Gly, reveal a further important point, namely that the vibrational spectrum is sensitive to subtle differences within a given structural motif. It is necessary to be aware of this dependence in making qualitative assignments of conformation from spectra. On the other hand, we can hope to utilize this sensitivity to obtain deeper insights into structure from the rigorous analyses of normal mode calculations.

This research was supported by NSF grants DMB-8816756 and DMR-8806975. We are indebted to A. Hempel, N. Camerman, and A. Camerman for performing the structure analysis on the new crystal form of Ala_3.

REFERENCES

1. Dzialoszynski, L. & Hofmann, T. (1973) *Biochim. Biophys. Acta* **302,** 406–410.
2. Fawcett, J. K., Camerman, N. & Camerman, A. (1975) *Acta Cryst. B* **31,** 658–665.
3. Hempel, A., Camerman, N. & Camerman, A. (1991) *Biopolymers,* preceding paper.
4. Krimm, S. & Bandekar, J. (1986) *Adv. Protein Chem.* **38,** 181–364.
5. Cheam, T. C. & Krimm, S. (1985) *J. Chem. Phys.* **82,** 1631–1641.
6. Dwivedi, A. M. & Krimm, S. (1982) *Macromolecules* **15,** 186–193.
7. Dwivedi, A. M. & Krimm, S. (1983) *Macromolecules* **16,** 340.
8. Jonsson, P. G. & Kvick, A. (1972) *Acta Cryst. B* **28,** 1827–1833.
9. Lehmann, M. S., Koetzle, T. F. & Hamilton, W. C. (1972) *J. Am. Chem. Soc.* **94,** 2657–2660.
10. Frey, M. N., Lehmann, M. S., Koetzle, T. F. & Hamilton, W. C. (1973) *Acta Cryst. B* **29,** 876–884.
11. Kerr, K. A., Ashmore, J. P. & Koetzle, T. F. (1975) *Acta Cryst. B* **31,** 2022–2026.
12. Bandekar, J. & Krimm, S. (1988) *Biopolymers* **27,** 885–908.
13. Cheam, T. C. & Krimm, S. (1989) *J. Mol. Struct.* **193,** 1–34.
14. Cheam, T. C. & Krimm, S. (1989) *J. Mol. Struct. (Theochem.)* **188,** 15–43.
15. Cheam, T. C. & Krimm, S. (1986) *J. Mol. Struct.* **146,** 175–189.
16. Sundius, T., Bandekar, J. & Krimm, S. (1989) *J. Mol. Struct.* **214,** 119–142.
17. Krimm, S. & Bandekar, J. (1980) *Biopolymers* **19,** 1–29.
18. Moore, W. H. & Krimm, S. (1976) *Biopolymers* **15,** 2465–2483.
19. Dwivedi, A. M. & Krimm, S. (1984) *J. Phys. Chem.* **88,** 620–627.
20. Bandekar, J. & Krimm, S. (1988) *Biopolymers* **27,** 909–921.
21. Krimm, S. & Dwivedi, A. M. (1982) *J. Raman Spectrosc.* **12,** 133–137.

Received July 18, 1990
Accepted September 14, 1990